Full Length Article

A novel dual ionization modality source for infrared laser ablation post-ionization mass spectrometry imaging to study fungicide metabolism and transport

Pieter C. Kooijman [a, b], Sybille Lamprecht [c], Marc Lamshoeft [c], Birte Beine [c], Bart J.H.T. Verhoeven [d], Shane R. Ellis [a], Ron M.A. Heeren [a, *]

[a] Maastricht University, Maastricht MultiModal Molecular Imaging Institute (M4I), 6229 ER, Maastricht, the Netherlands
[b] TI-COAST, 1098 XH, Amsterdam, the Netherlands
[c] Bayer AG, Research and Development, Crop Science, Monheim Am Rhein, 40789, Germany
[d] Maastricht University, Instrument Development, Engineering and Evaluation (IDEE), 6229 ER, Maastricht, the Netherlands

ARTICLE INFO

ABSTRACT

We present a novel probe design for ambient laser-based mass spectrometry imaging combining electrospray ionization (ESI) and atmospheric pressure chemical ionization (APCI) in a single probe, compatible with a commercial laser ablation electrospray ionization (LAESI) instrument. Here we describe the probe design considerations and features, as well as an in-house developed data processing routine designed to extract accurate mass spectrometry imaging data from ambient laser ablation post-ionization experiments. We characterize the probe performance in both APCI and ESI mode on a selection of compounds and show improved pixel-to-pixel repeatability for LA-APCI as compared to LAESI. We apply the dual ionization probe in APCI mode in a time series experiment to monitor agrochemicals on tomato plants. We investigate the translocation of fungicide isotianil and one of its metabolites, anthranilonitrile, by mass spectrometry imaging over a period of two weeks after application on a leaf surface. LA-APCI-MSI shows translocation of anthranilonitrile from treated leaves towards non-treated leaves. In summary, we demonstrate that LA-APCI imaging is a valuable addition to the ambient mass spectrometry toolbox, with particular advantages for imaging experiments across a variety of compounds.

1. Introduction

In recent years, mass spectrometry imaging (MSI) has proven itself as a valuable tool to uncover the spatial distribution of biologically relevant compounds [1] either in a targeted [2–4] or untargeted [5–8] approach. The scope of samples and compounds compatible with MSI has grown considerably as the technology has matured. Key driving force behind these developments has been matrix-assisted laser desorption ionization (MALDI) MSI [9]. MALDI offers superior sensitivity for many compounds and high spatial resolution (down to ~1 μm) [10]. MALDI relies on surface extraction of analytes through the application of an UV absorbing matrix onto the sample surface, typically a thin tissue section. For many sample types, most notably animal or human tissue sections, MALDI has proven immensely powerful [11], but for plant material it is difficult to retain morphological information in this manner. Plant material contains a significant amount of water that makes it poorly compatible with most MALDI instruments that analyse the sample *in vacuo*. Desorption Electrospray Ionization (DESI) has been shown to efficiently sample the outer surface of a plant leaf, but does not penetrate the subsurface layer [12]. An approach for the analysis of plant material is needed, capable of direct sampling both the surface as well as the subsurface layers - without need for extensive sample preparation - under ambient pressure conditions.

1.1. LAESI-MSI

Many efforts have focussed on the development of ambient infrared laser-based sampling techniques coupled with a separate ionization step. The most developed of these techniques is called

laser-ablation electrospray ionization (LAESI) [13] (or infrared matrix-assisted laser desorption electrospray ionization (IR-MAL-DESI) [14]). This molecular imaging technique has been developed to analyse biologic surfaces in their native state in an ambient environment (i.e. at atmospheric pressure). The infrared laser ablation wavelength of 2.94 μm in these experiments is chosen to couple directly to the hydroxyl vibrations of water in biological samples. The coupling of the IR laser desorption step to ESI enables us to locally detect a wide range of compounds, including the generation of multiply charged intact proteins [15]. This is challenging with MALDI-MSI. LAESI-MS has been used in the past to perform analysis on plants [16−18], tissue sections [14,19] and bacterial colonies [20,21] amongst others.

Drawbacks mentioned for this technique are a relatively low throughput [15], moderate spatial resolution (commonly performed at 100−250 μm spatial resolution) [22,23] and electrospray ionization is poorly suited for the analysis of non-polar compounds [24,25]. Another inherent drawback of the commercial LAESI geometry is limited repeatability (both pixel-to-pixel and between experiments). Electrospray ionization efficiency relies on a stable and constant electrospray plume, while each laser desorption event in LAESI introduces a potential disturbance. Several groups have optimized experimental LAESI parameters to improve the stability of imaging experiments [21,26,27].

This paper describes a new ionization probe that addresses two of these drawbacks: the analyte electronegativity range and the repeatability of measurements. The ionization probe design that we describe is somewhat similar to the design idea of the dual ESI and APCI source introduced by Cheng et al. [28]. The design has been adapted significantly to be compatible with LAESI instrumentation. The probe enables atmospheric pressure chemical ionization (APCI), based on a dielectric barrier discharge (DBD) principle, without sacrificing the ability to utilise ESI-based post-ionization. DBD relies on the generation of charged species in a noble gas plasma environment. When in contact with atmospheric gases a cascade of charge-exchange reactions leads to analyte ionization under ambient conditions. This principle works well for a broad range of compounds, being more effective in ionizing non-polar compounds than electrospray ionization [24,25]. We have performed a general characterization of the system performance, looking specifically at the instrument sensitivity for several compound classes, as well as the pixel-to-pixel repeatability of both ionization techniques.

In this work we describe the application of the dual ionization probe in a study to visualize the distribution of the fungicide isotianil (IST), one of its metabolites and native compounds in leaves of the tomato plant (Solanum lycopersicum) over time. Isotianil is a novel fungicide belonging to the group of plant defence modulators/inducers (FRAC Group P) as it induces systemic acquired resistance in plants. Isotianil is particularly effective to control rice blast and bacterial leaf blight. It is also active against some leaf spot diseases, powdery mildews, as well as against bacterial diseases like Pseudomonas sp. and Xanthomonas sp.. [29]. In contrast to most plant activators, isotianil is a prodrug which is slowly converted into the active compound, DCIT-acid, and anthranilonitrile (ANT) [30] (see Fig. 1). Isotianil supposedly remains at the deposition site on top of the leaf surface, working as a depot by slowly releasing the active compound. In search of new applications for isotianil it is of great interest to obtain information on the interaction with and distribution through target crops of the pro-drug and its metabolites. For instance, the rate of metabolization of isotianil is crop specific and of great influence on the efficacy of isotianil as a fungicide. Earlier studies to answer these questions have employed autoradiography to monitor the distribution of ^{14}C or ^{15}O radio-labelled compounds through leaves [31]. This technique is sensitive
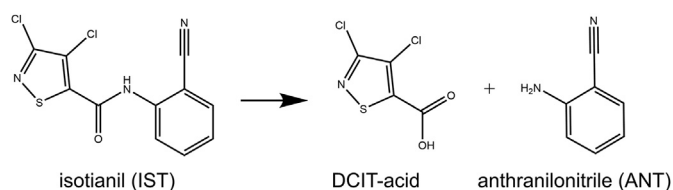

Fig. 1. Isotianil metabolism route to the active compound DCIT-acid and anthranilonitrile.

and can monitor a large sample area without sample preparation. However, autoradiography can only be applied in a targeted manner and cannot distinguish between the initial labelled molecule and possible metabolites. It requires the time-consuming and expensive synthesis of radiolabelled compounds and does not provide information on endogenous compounds in the sample. MSI based approaches in the ambient environment can investigate the distribution of a variety of plant-based molecules, agrochemicals and their metabolites without the use of any radiolabels. We designed a timeseries MSI experiment on isotianil treated leaves using the LA-APCI mode of our novel ionization probe to investigate the translocation of IST and its metabolites over time.

2. Materials and methods

2.1. LAESI-MS system

All experiments were performed using a modified Protea DP-1000 LAESI system (Protea Biosciences, US) coupled to a Thermo Q-Exactive mass spectrometer (Thermo Scientific, Bremen, DE), unless stated otherwise in the text. The DP-1000 LAESI system was equipped with an external inlet capillary heater, set to 190 °C for all experiments, and a 2194 nm 10 Hz IR OPO laser with a fixed focal length of 50 mm. The resulting laser spot size was approximately 200−250 μm, with a step size of 250 μm for all imaging experiments. The sample stage was cooled to 4 °C and the sample bay was continuously flushed with nitrogen gas for all experiments to maintain the sample water content during analysis [32]. The mass spectrometer was operated at a set mass resolution of 17500, m/z range of 100−350 and an injection time of 20 ms for the LA-APCI time series imaging experiments. The high mass resolution imaging experiments were performed with a resolution setting of 120,000 at m/z 200, with 820 ms injection time. The MS inlet capillary temperature was set to 190 °C, the S-lens level to 50 arb. units. For the limit-of-detection (LOD) measurements the mass range was kept at m/z 100−550 for all experiments.

2.2. Chemicals

Isopropyl alcohol, acetonitrile, water, HPLC-grade methanol and formic acid 99% were purchased from Biosolve B.V. (Valkenswaard, The Netherlands). Ethylene glycol, cholesterol, verapamil hydrochloride, sodium taurocholate hydrate, atrazine, anthranilonitrile were purchased from Sigma Aldrich Chemie Gmbh, Germany. Fluopyram and isotianil standards were supplied by Bayer AG, Crop Science, Germany. Argon gas (5.0 purity) was purchased from Linde Gas.

2.3. Dual modality ionization probe

The dual modality ionization probe was designed to replace the original ESI probe from the DP-1000 unit. The probe is fully interchangeable with the standard probe of the DP-1000 unit and requires no changes to experimental parameters - when operated in

the LAESI mode - compared to the original probe. The dual modality ionization probe features a radial DBD design, surrounding the coaxially placed ESI emitter. The basic concept of the new dual modality probe is shown in Fig. 2 and an additional schematic design and photo is added in Figure S1. Our design deviates from the design presented by Cheng et al. [28] in several ways: (1) the addition of a metal electrospray emitter and consequential insulation between the APCI ground electrode and the electrospray emitter; (2) the miniaturisation of the whole system to fit parallel to the sample at the correct height offset; (3) the addition of a PTFE glass nozzle to focus the gas stream; and (4) the addition of thermal and electric insulation of the probe to protect the sample integrity. The dual ionization probe can be operated in two modes, either APCI or ESI. Switching between LAESI and LA-APCI mode takes approximately 60 s, plus time for electrospray stabilization.

In APCI mode, argon gas is fed into the DBD chamber (entering Fig. 2 from the left). An RF potential (input voltage 30 V, 30.7% duty cycle and 90.0 kHz output) was applied to the copper outer electrode by a G2000 power supply (Redline Technologies, Baesweiler, DE) and tuned to the lowest RF amplitude that would sustain a stable discharge (approx. 1 kV peak-to-peak in our experiments). The quartz dielectric barrier limits the discharge current to the central, grounded, stainless-steel counter electrode. A PEEK sleeve insulates the grounded electrode from the coaxially placed stainless steel Metal TaperTip emitter (320 μm o.d., 100 μm i.d., New Objective, Woburn, MA, USA). A $+700$ V or -700 V DC potential was placed on the emitter for MS analysis in positive or negative mode, respectively. The gas flow rate of Argon 5.0 was controlled by a flow controller (Bronkhorst, Veenendaal, NL) at 50 mL min^{-1}, which was determined to be optimal for this setup.

In ESI mode, the probe works similarly to the original LAESI DP-1000 probe (e.g. the same electrospray emitter) and has the same overall geometry. In this mode, up to 1 L min^{-1} of nitrogen sheath gas flows through the quartz tube, exiting parallel to the electrospray emitter. The optimal operational parameters for ESI mode depend on the application and are comparable to the standard DP-1000 system. We have chosen to use settings commonly used in literature [18,20,33] for the experiments shown here: 4000 V DC potential with a solvent flow rate of 1.2 μL min^{-1} 1:1 methanol/water + 1% (v/v) formic acid in positive mode. 2700 V DC potential with a solvent flow rate of 1.2 μL min^{-1} 2:1 methanol/chloroform +0.1% (v/v) acetic acid in negative mode.

2.4. Experimental procedures

2.4.1. Source characterization

Sensitivity measurements were performed on standards following a protocol adapted from Vertes and Anderton (see Protocol S1) both for LAESI and LA-APCI. Most notably, 1:1 isopropyl alcohol:ethylene glycol (v:v) was used as a solvent to promote solubility of less polar compounds and reduce adverse effects from evaporation and surface tension.

Fluopyram, cholesterol, atrazine and anthranilonitrile were individually diluted in 1:1 isopropyl alcohol/ethylene glycol to form dilution series ranging from 100 μM to 50 nM. Verapamil and taurocholic acid were diluted in the same solution to form concentration series ranging from 10 μM to 500 pM, because these compounds are known to be easily detected in LAESI. The isotianil dilution series (100 μM−50 nM) was prepared in 1:1 isopropyl alcohol/ethylene glycol, though it should be noted that isotianil proved difficult to dissolve in all IR-laser compatible solvents that we tested. All compounds, except taurocholic acid were measured in positive mode, for both ESI and APCI mode. 10 μL was spotted onto a Protea 96-well target plate for each standard and
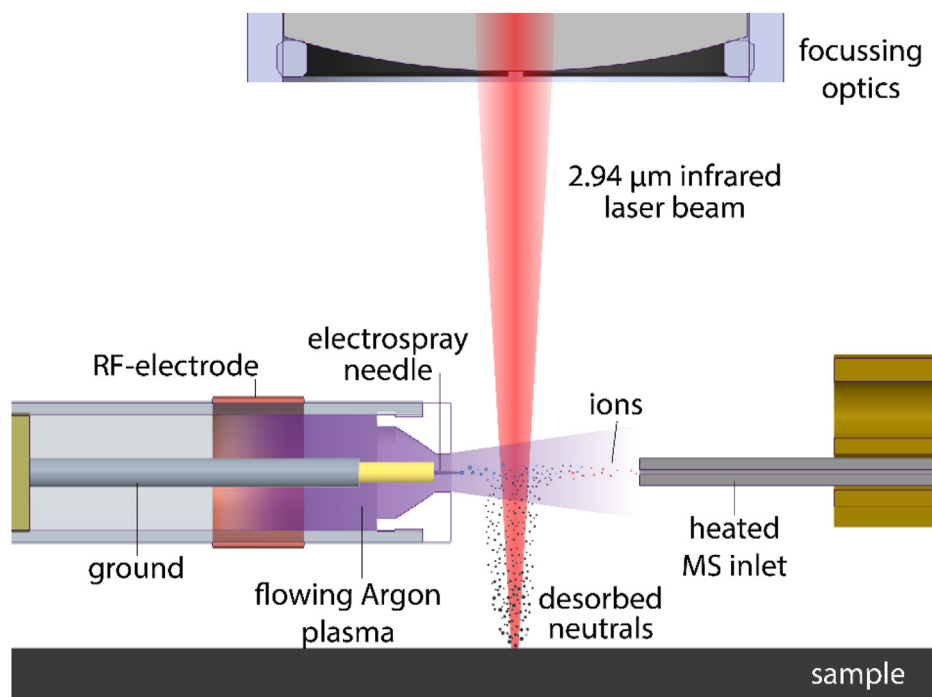

Fig. 2. Schematic representation of LAESI/LA-APCI geometry. The main components of the dual ionization probe are shown (left), the mass spectrometer inlet (right), the laser and focussing optics (above) and the sample (below). Upon a laser ablation event, neutral particles are released into the void between the ionization probe and the mass spectrometer inlet. Here, the neutrals receive a charge from either the electrospray nebula or the APCI gas stream. The constant electric field gradient between the ionization probe and MS inlet drives the analyte ions towards the mass spectrometer inlet.

concentration. Each well was irradiated with 10 shots at 70% laser power (0.8 mJ, σ ≈ 1%) and 10 Hz in sequence from low to high concentration. The full sequence was repeated three times on the same target plate.

To determine the signal-to-noise ratio for each analyte, the average peak intensity was determined per experiment (36 scans averaged) by a custom Matlab script. The LOD and LOQ were determined as 3 and 10 times the standard deviation of the noise, respectively. The average noise level was provided by the Xcalibur software package (Thermo Scientific Inc., San Jose, US).

2.4.2. Fungicide detection in plant leaves

Tomato plants were supplied and treated by Bayer Crop Science. On day 0 multiple leaves were spotted with 5 times 10 μL of fungicide formulation (Bayer AG, Monheim, DE) (250 ppm isotianil) directly the base of the leaf and left to dry. For each time point leaves were collected, individually packed in air-tight zip-lock bags and kept frozen at −20 °C until analysis. In addition, leaves were collected that were not treated, but were on the same plant as a treated leaf (which we refer to as 'distal leaves'). The sample was left to thaw while packed shortly prior to analysis. Thawed, the leaf was transferred onto a plain glass slide (top-side up) and inserted into the sample bay and kept at 4° Celsius. For each sample, a region containing approx. 7000 pixels was selected covering both the leaf base and the tip of the leaf. Each position was irradiated 6 times, at 5 Hz and 70% laser power (1.1 J/cm^2) followed by 2 s of dwell time. The sample is fully penetrated for both LAESI and LA-APCI using these settings.

The method used to prepare the samples for the high mass resolution experiments (Section 3.5) and Figures S3, S4 and S5 is slightly different. The leaves were washed by immersion in 80% acetonitrile solution directly after harvesting. After drying the samples were mounted onto a glass slide using double sided tape. The samples were subsequently analysed immediately after mounting, alleviating the need for cryostorage and thawing.

2.5. Data processing strategy

A data processing strategy was developed in-house to handle continuously recorded, pulsed extraction imaging experiments on ion trap-based systems (e.g. FT-ICR or Orbitrap). In most post-ionization experiments, acquisition of mass spectral data occurs independent from the laser ablation event. Therefore, spectra need to be identified, assigned to a given sampling position, and extracted for data processing. We developed a spectral extraction algorithm in MATLAB (MathWorks, Inc., Natick, USA) based on the ChemomeTricks platform [34]. This algorithm relies on two key parameters: (1) a source trigger pulse recorded in parallel with the mass spectral data on an analog input channel and (2) the extracted ion chromatogram of one predefined sample related peak. The correct spectral number for each pixel is automatically determined by correlating the source trigger pulses to peaks in the extracted ion chromatogram. The spectral summation window width and image size information (step size, x/y-dimensions) are based on analysis parameters extracted from LAESI DP-1000 metadata. In addition, the algorithm determines the mass spectral bin width across the spectrum, based on the data acquisition rate, and corrects for possible missing or erroneous triggers. The peak-picked imaging dataset is then exported to the ChemomeTricks [34] data format and imzML. All mass spectrometry images shown are plotted on a linear intensity scale using the *viridis* colormap [35], with TIC normalization and scaled to the 99.9th percentile. The *viridis* colormap has been proposed as a 'fair', representative, and colour-blind friendly alternative to other commonly used colormaps in MSI [36].

3. Results and discussion

3.1. LA-APCI ionization principle

When the source is operated in APCI mode, an argon plasma is created in the chamber via a Townsend-type discharge. The argon plasma mixes with atmospheric air near the exit of the probe, upon which a charge transfer cascade ionizes laser desorbed neutrals in a manner analogous to traditional APCI approaches. The electric field gradient between the probe and the MS inlet enhances (~10-fold signal increase) the sensitivity of the source by directing positively charged particles towards the MS inlet, without significantly altering the observed ions. The most abundantly observed species in APCI mode are singly (de)protonated ions, though radical ions (~3% of the singly protonated peak intensity) and ammonium adducts (<30% of the singly protonated) can also be observed.

3.2. Source characterization

In order to characterize the performance of the probe we determined the limit-of-detection (LOD), limit-of-quantitation (LOQ) and repeatability (determined as relative standard deviation (RSD)) on seven compounds in both ESI and APCI mode. The results are summarized in Table 1.

Table 1 shows that the LAESI and LA-APCI modes have comparable sensitivities for fluopyram, anthranilonitrile and taurocholic acid. LAESI shows higher sensitivity for cholesterol and verapamil, and to a lesser extent atrazine. In all cases except cholesterol - in which LA-APCI sensitivity was significantly lower − the LA-APCI results have less variation (lower RSD values) than the LAESI data, thus having better pixel-to-pixel repeatability. Our observations suggest this is due to frequent disturbances of the electrospray plume by laser ablation events in LAESI experiments. Visual observations have shown ablated material and/or pressure wave effects cause the electrospray regime to alter temporarily which induces spray instabilities. This influences the ionization efficiency for subsequent laser ablation events. LA-APCI, which relies on an ionized gas flow, suffers significantly less from these effects because the generation of reactive species in the DBD chamber is not affected by ablation events. Most of the remaining variation in our LA-APCI measurements is presumed to originate from variation in the laser ablation event itself.
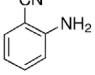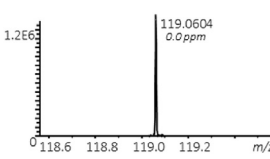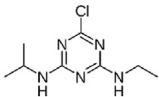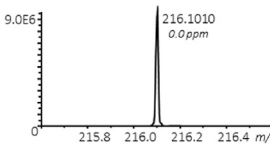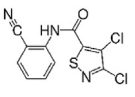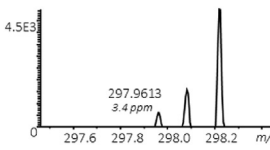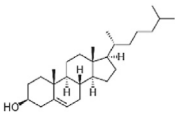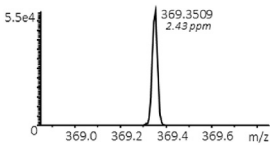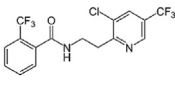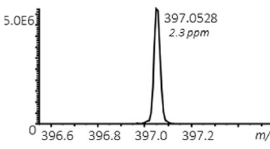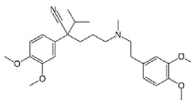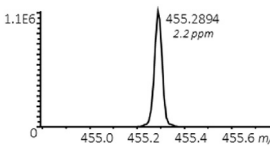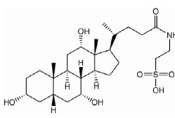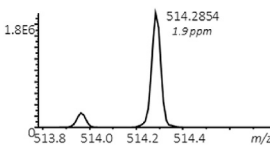
Calibration curves were generated for all compounds (included in Figure S2), except for isotianil. Isotianil dissolved poorly in all IR-laser compatible solvents that we considered for this experiment, due to its strong hydrophobic character. This characteristic also makes isotianil a prime candidate for APCI-based ionization. In this source characterization study no signal was obtained from isotianil with LAESI. We were able to obtain a spectrum with LA-APCI but only at a 100 μM concentration. This spectrum could have been produced from non-dissolved particulate matter. From the isotianil distribution studies (below) however, we have observed LA-APCI to be quite sensitive to detect isotianil on a leaf surface, in contrast to LAESI. In the following section, we will demonstrate how LA-APCI MSI can be used to monitor the isotianil distribution and the distribution of one of its metabolites on a plant surface.

3.3. Visualizing the translocation of fungicide isotianil and one of its metabolites in tomato leaves

Next, we investigated the ability of LA-APCI-MSI to visualize the translocation of the isotianil distribution after its local application to the base of a tomato leaf. We were able to simultaneously image several endogenous molecular species and metabolites of isotianil. The isotianil metabolite anthranilonitrile (ANT) distribution was

Table 1

An overview of all compounds monitored in the source characterization protocol and their respective LOD, LOQ and RSDs for LAESI and LA-APCI.

Compound	Structure	Observed species	Spectrum		LOD	LOQ	RSD
Anthranilonitrile (ANT) $M_{mi} = 118.05$ gmol^{-1}		[M+H]$^+$: 119.0604		LAESI LA-APCI	486 nM 391 nM	1.54 μM 1.53 nM	1.08 0.434
Atrazine $M_{mi} = 215.09$ gmol^{-1}		[M+H]$^+$: 216.1010 [M]$^{a+}$: 215.0938		LAESI LA-APCI	12.2 nM 46.8 nM	50.7 nM 139 nM	0.637 0.445
Isotianil (IST) $M_{mi} = 296.95$ gmol^{-1}		[M+H]$^+$: 297.9603		LAESI LA-APCI	- -	- -	- -
Cholesterol $M_{mi} = 386.35$ gmol^{-1}		[M − OH]$^+$: 369.3516		LAESI LA-APCI	2.47 μM 22.2 μM	7.08 μM 51.7 μM	1.09 1.23
Fluopyram $M_{mi} = 396.05$ gmol^{-1}		[M+H]$^+$: 397.0537		LAESI LA-APCI	27.0 nM 33.0 nM	102 nM 119 nM	0.516 0.494
Verapamil $M_{mi} = 454.28$ gmol^{-1}		[M+H]$^+$: 455.2904		LAESI LA-APCI	13.0 nM 29.7 nM	40.3 nM 97.5 nM	0.868 0.558
Taurocholic acid $M_{mi} = 515.29$ gmol^{-1}		[M − H]$^-$: 514.2844		LAESI LA-APCI	47.0 nM 52.7 nM	156.6 nM 181.1 nM	0.815 0.805

[a] Table 1 shows the compound structure, monoisotopic mass, observed species, limit-of-detection, limit-of-quantitation and relative standard deviation. The mass spectra are averages of a single measurement point of the highest concentration of each compound. All spectra shown are 1 Th wide.

also subject of study. Leaves were harvested from the plant 2, 4, 7, 11 and 14 days after local application of isotianil formulation at the base of each leaf, and measured after cryostorage. The control specimen, harvested on day 0 without application of the fungicide formulation exhibited no isotianil or ANT signal. Fig. 3 shows the translocation of isotianil and ANT during the course of this experiment. A fragment of phenylalanine (2-phenyl-ethenamine), a confirmed tomato plant endogenous amino acid [37], was monitored as a reference molecule to visualize the leaf surface (Fig. 3c). The identity of 2-phenyl-ethenamine was confirmed through a separate experiment (data not shown). The LA-APCI images shown in Fig. 3 took between 6 and 9 h to acquire per leaf.

The isotianil images show that this compound is still fixed on its application site, even after 14 days. The highest TIC normalized signal intensity is visible on the first measurement day, gradually diminishing in average normalized signal intensity to 50% by day 14. This allows us to estimate the metabolic rate of isotianil in

tomato leaves. Fig. 3 shows anthranilonitrile is most abundant at the application site, with a similar pattern to that of isotianil. In contrast, Figure S3 shows homogenous distributions of anthranilonitrile over the entire tomato leaves. These leaves have been washed prior to analysis (see Section 2.4.2) and therefore contain only trace amounts of isotianil on the surface, with most of the isotianil still present absorbed into the leaf tissue. The leaves of Fig. 3 have been frozen and thawed with the isotianil residue still on the leaf surface and thus contain a much higher concentration. This leads us to believe the most intense anthranilonitrile signal in Fig. 3 is in fact a laser fragmentation product of isotianil, as opposed to a metabolite.

The anthranilonitrile signal - normalized to the TIC — in the leaf surrounding the application area rises steadily, from ~1.5e-3 on day 2 to ~5e-3 on day 14. Fig. 3d shows the ratio between the anthranilonitrile and isotianil signal intensities — summed for the entire image area. This ratio shows the relative concentration of
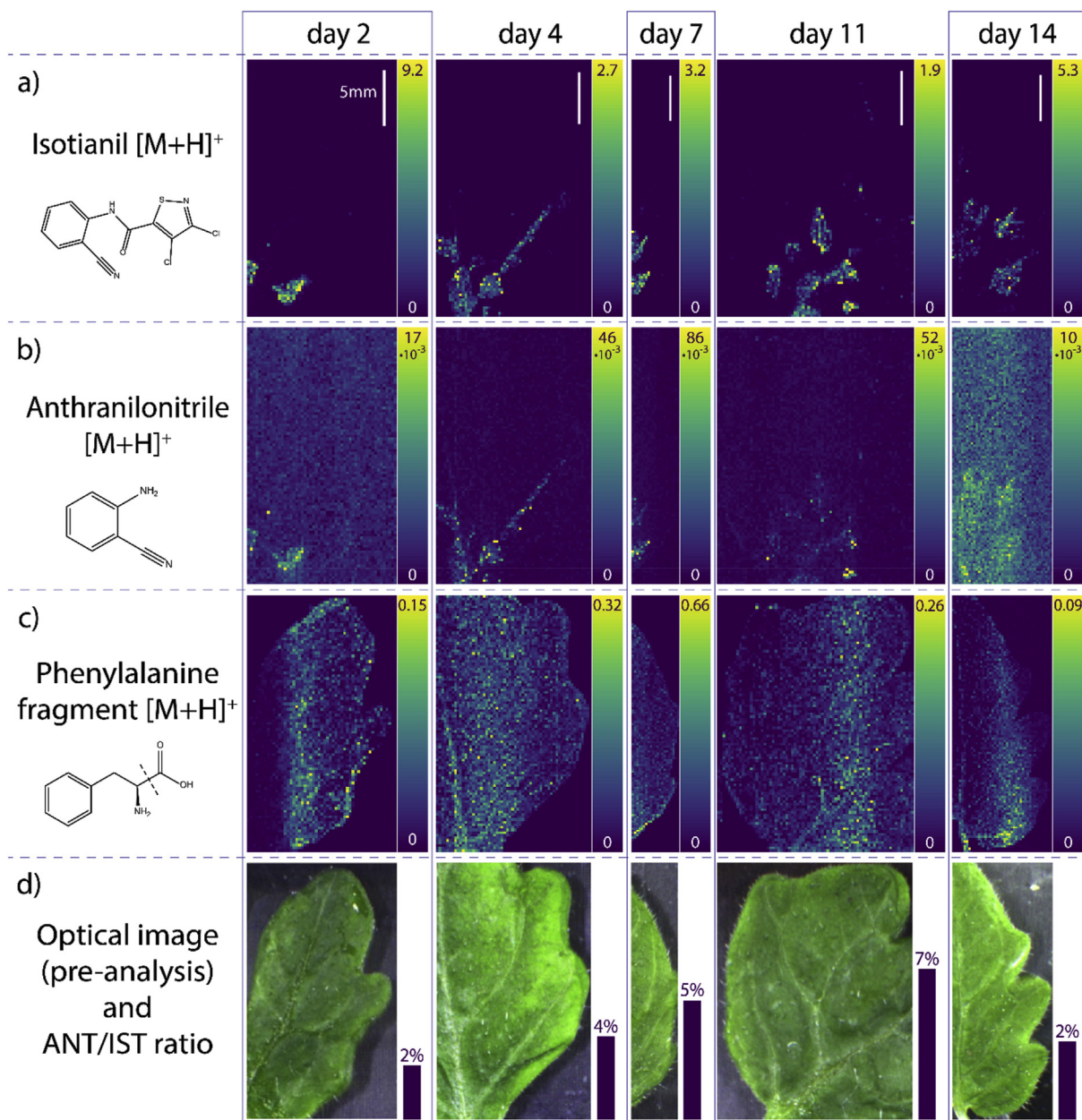
Fig. 3. Timeseries showing the distribution of isotianil (IST) (a) and its metabolite anthranilonitrile (ANT) (b) using LA-APCI mass spectrometry imaging. Leaves treated locally at the base with IST were harvested 2, 4, 7, 11 and 14 days after application and measured after cryo-storage. The control specimen, harvested on day 0, without application of the fungicide formulation exhibited no IST or ANT signal. The distribution of the phenylalanine fragment 2-phenyl ethenamine is (c) and the pre-analysis optical images (d) are added for reference. The ratio between the total summed anthranilonitrile and isotianil signals is plotted in d).

anthranilonitrile increases up to day 10, before receding at day 14. We therefore conclude that - as isotianil is converted over time - anthranilonitrile distributes throughout the tomato leaves.

Interestingly, we are able to obtain very high signal-to-noise ratios (up to S/N 3000) on isotianil desorbed from the leaf surface (Fig. 3), in contrast to the LA-APCI LOD results. We conclude isotianil is not a suitable compound for liquid based limit-of-detection measurements in IR-laser setups. As an approximation we can use the amount of isotianil applied as a reference to estimate the sensitivity of our setup. A single pixel of the application area should contain approximately 280 pmol of isotianil, which should theoretically yield an LOD of 450 nmol cm^{-2}.

3.4. ANT distribution is distal leaves

So far, we investigated the translocation behaviour of IST and ANT within the leaf upon which IST was applied. For the effectiveness of a fungicide it is equally important if and how the fungicide translocates to other parts of a plant. We harvested untreated leaves from tomato plants carrying several treated leaves at three time points: day 0, day 3 and day 14. Fig. 4 shows the translocation of the compounds over time in these "distal" leaves. Isotianil is not detected in any of the distal leaf samples, proving that isotianil stays immobilized at the application site. Anthranilonitrile was not detected in the control sample harvested on day 0,
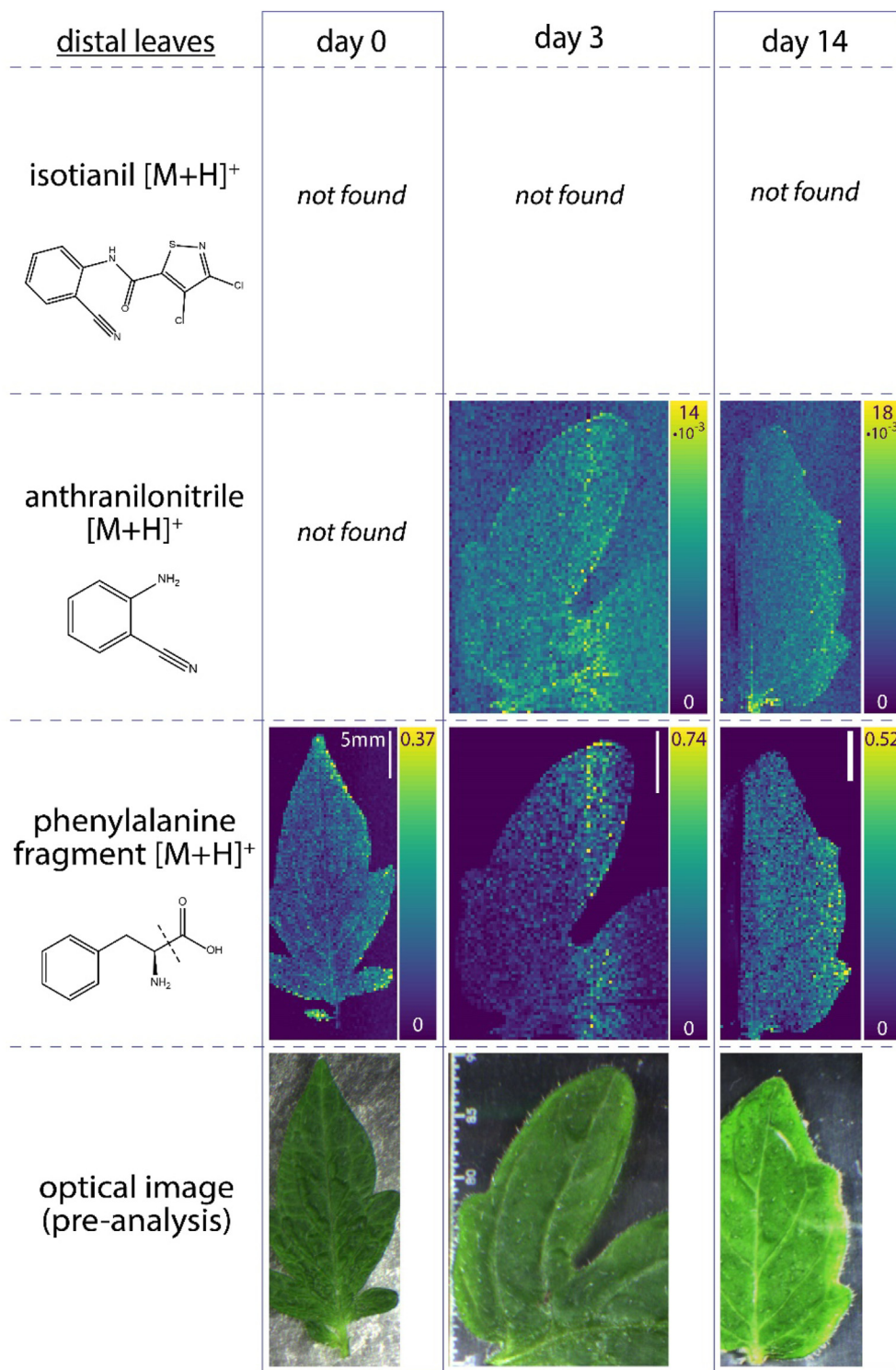
Fig. 4. Mass spectral images of anthranilonitrile detected in a distal leaf of a treated plant 3 and 14 days after application. Isotianil was not detected in any of samples. The leaf harvested on day 0 - before treatment of the plant - shows no signal for either isotianil or anthranilonitrile. The distribution of endogenous metabolite phenylalanine and the optimal images are added for reference. All images are plotted on a linear scale and TIC normalized.

but was detected with a TIC normalized signal intensity of ~7e-3 and ~11e-3 in the day 3 and day 14 samples, respectively. This is markedly higher than the signal intensity found outside the application area of the treated leaf, demonstrating translocation of anthranilonitrile from treated leaves towards non-treated leaves. Phenylalanine fragment MS images and the optical images are added for reference.

3.5. High resolution LA-APCI imaging confirms compound identity

We repeated our imaging experiment on a Thermo Orbitrap Elite system with high mass resolution to confirm our compound assignments through accurate mass measurements and MS/MS. The accurate mass measurements are shown in Fig. 5.

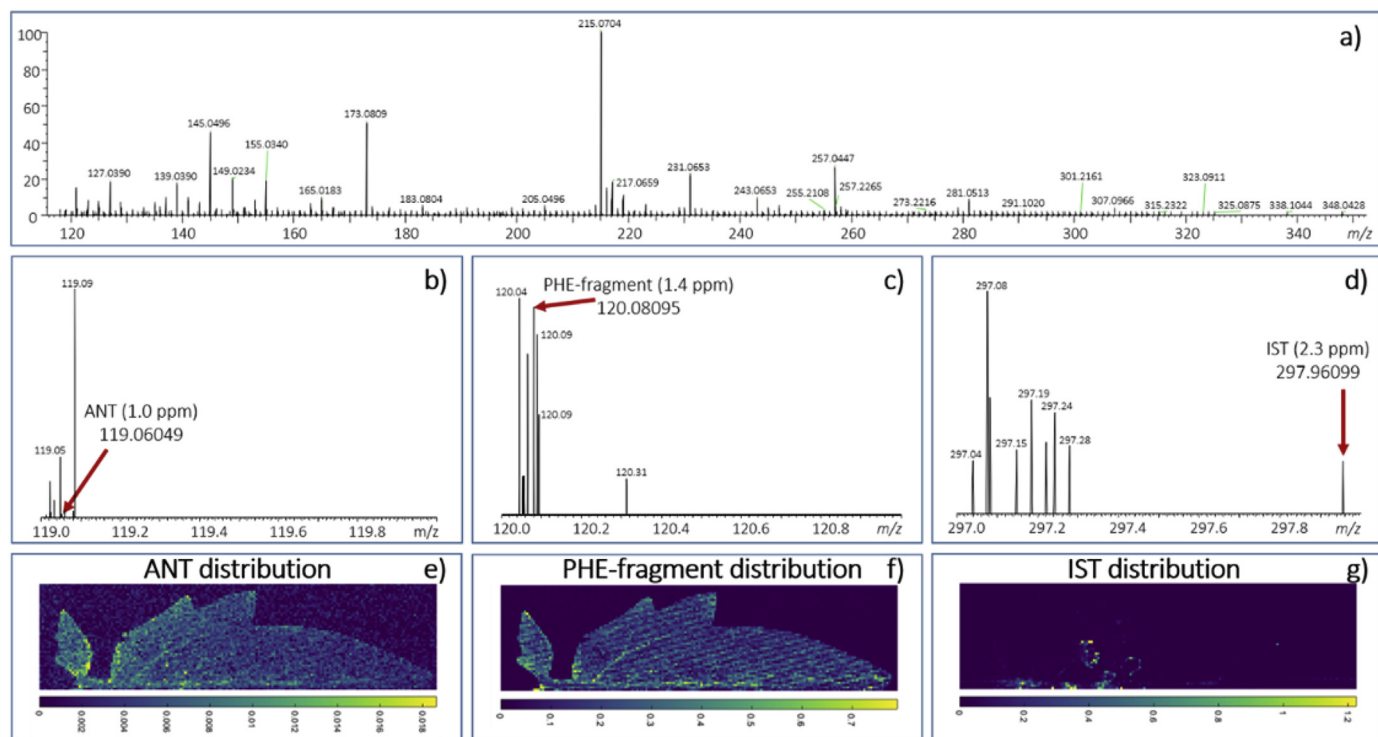Fig. 5a is a single pixel spectrum from this experiment. LAESI

Fig. 5. High mass resolution Orbitrap based LA-APCI imaging experiment on an isotianil (IST) treated tomato leaf, harvested at day 9. a) Single pixel spectrum over the entire mass range 118−305 *m/z*. b) Anthranilonitrile (ANT) range extracted from A 119−120 *m/z*. c) Phenylalanine (PHE)-fragment range extracted from A 120−121 *m/z*. d) IST range extracted from A 297−298 *m/z*. Red arrows indicate the exact mass peak at which images in e), f), g) are generated, that show the distribution of ANT, PHE-fragment and IST respectively derived from the Orbitrap imaging experiment. The total imaging area is 43.3 × 11.5 mm.

spectra (and in fact most ambient desorption techniques) and LA-APCI spectra contain a significant amount of background ions. These background ions could originate from solvent contaminants, laboratory air contaminants or other sources. As can be seen in Fig. 5b−d our single pixel spectra contain some interfering compounds, that require high mass resolution to resolve. With a mass resolution of 120,000 it is possible to create mass spectral images with high contrast, even for low intensity compounds in the presence of isobaric interferences. This comes at a price of time, taking 11 h to record the images shown in Fig. 5e−g. With longer total mass spectrometer scan times (in this case 1.38 s, with a C-trap injection time of 820 ms) the period that the C-trap is not accumulating ions can become significant (i.e. low duty cycle), and can coincide with laser ablation events. The periodic loss of analyte ions results in a pattern of analyte ion intensity dips. This effect is visible in Fig. 5f as a striped pattern embedded in the image. None the less, mass spectrometry imaging can measure endogenous compounds and target molecules simultaneously, as demonstrated in Figure S4 for a tomato leaf and Figure S5 for a grapevine leaf. LA-APCI can generate high quality, crisp mass spectral images if both high selectivity (either by mass resolution, MS/MS or ion mobility) and a high duty cycle are provided, as shown in Figures S4 and S5.

3.6. Combined ESI and APCI post-ionization

Finally, we investigated the possibility to perform both ESI and APCI at the same time. The combination of APCI and ESI mode was found to be feasible and generates molecular ion species characteristic for either mode simultaneously. However, the parameter range suitable for simultaneous APCI and ESI mode does not match the optimal parameter range of either of the modes when used

separately. Consequently, the sensitivity of the system in combined mode is significantly reduced. A better alternative is to perform ESI and APCI mode MSI imaging in sequence. Switching between ESI and APCI mode is relatively fast, in the order of seconds, though both ionization modes require some time to stabilize after initialization (5−10 min). Therefore, switching between modes in between pixels is not feasible. However, APCI and ESI mode images can be recorded in sequence on the same sample area if a larger grid size is chosen and a one-pixel offset is used between the images.

4. Conclusion

We have designed and tested a novel ionization probe for ambient IR-laser based desorption mass spectrometry combining both ESI and APCI modalities for use in a LAESI-MS imaging platform. ESI mode proved more sensitive for some tested compounds, whereas APCI mode was more sensitive for isotianil. Overall, APCI mode showed a higher pixel-to-pixel repeatability. We argue this is due to the nature of dielectric barrier discharge − suffering less from ablation event disturbances than ESI mode. This is corroborated by our observations in imaging experiments, in which LA-APCI imaging is more robust and contains significantly less instrumental variation compared to LAESI imaging experiments. We have tested our new approach for the investigation of plant-based metabolism of agrochemicals and endogenous molecules on plant leaf surfaces. We were able to visualize the translocation behaviour and metabolism of isotianil in tomato plants over time, while simultaneously monitoring endogenous compounds. The method presented here has added analytical value for agrochemical studies and ambient imaging applications in general.

CRediT authorship contribution statement

Declaration of competing interest

Acknowledgements

Appendix A. Supplementary data

Supplementary data to this article can be found online at https://doi.org/10.1016/j.ijms.2021.116602.

References

[1] K. Chughtai, R.M.A. Heeren, Mass Spectrometric Imaging for biomedical tissue analysis, Chem. Rev. 110 (2010) 3237−3277, https://doi.org/10.1021/cr100012c.

[2] C. Giesen, et al., Highly multiplexed imaging of tumor tissues with subcellular resolution by mass cytometry, Nat. Methods 11 (2014) 417−422, https://doi.org/10.1038/nmeth.2869.

[3] M. Angelo, et al., Multiplexed ion beam imaging of human breast tumors, Nat. Med. (2014) 436−442, https://doi.org/10.1038/nm.3488 (N. Y., NY, U. S.).

[4] F.P. Barre, et al., Derivatization strategies for the detection of triamcinolone acetonide in cartilage by using matrix-assisted laser desorption/ionization mass spectrometry imaging, Anal. Chem. 88 (2016) 12051−12059, https://doi.org/10.1021/acs.analchem.6b02491.

[5] B. Balluff, M. Hanselmann, R.M. Heeren, Mass spectrometry imaging for the investigation of intratumor heterogeneity, Adv. Canc. Res. 134 (2017) 201−230, https://doi.org/10.1016/bs.acr.2016.11.008.

[6] B. Heijs, et al., Multimodal mass spectrometry imaging of N-Glycans and proteins from the same tissue section, Anal. Chem. 88 (2016) 7745−7753, https://doi.org/10.1021/acs.analchem.6b01739.

[7] J.M. Spraggins, et al., MALDI FTICR IMS of intact proteins: using mass accuracy to link protein images with proteomics data, J. Am. Soc. Mass Spectrom. 26 (2015) 974−985, https://doi.org/10.1007/s13361-015-1147-5.

[8] S.R. Ellis, et al., Automated, parallel mass spectrometry imaging and structural identification of lipids, Nat. Methods 15 (2018) 515−518, https://doi.org/10.1038/s41592-018-0010-6.

[9] M. Stoeckli, T.B. Farmer, R.M. Caprioli, Automated mass spectrometry imaging with a matrix-assisted laser desorption ionization time-of-flight instrument, J. Am. Soc. Mass Spectrom. 10 (1999) 67−71, https://doi.org/10.1016/S1044-0305(98)00126-3.

[10] B. Spengler, M. Hubert, Scanning microprobe matrix-assisted laser desorption ionization (SMALDI) mass spectrometry: instrumentation for sub-micrometer resolved LDI and MALDI surface analysis, J. Am. Soc. Mass Spectrom. 13 (2002) 735−748, https://doi.org/10.1016/S1044-0305(02)00376-8.

[11] F. Dewez, et al., Precise co-registration of mass spectrometry imaging, histology, and laser microdissection-based omics, Anal. Bioanal. Chem. 411 (2019) 5647−5653, https://doi.org/10.1007/s00216-019-01983-z.

[12] C. Janfelt, in: He Lin (Ed.), Mass Spectrometry Imaging Of Small Molecules Vol. 1203 Methods In Molecular Biology, Humana Press, 2015, pp. 91−97.

[13] P. Nemes, A. Vertes, Laser ablation electrospray ionization for atmospheric pressure, in vivo, and imaging mass spectrometry, Anal. Chem. 79 (2007) 8098−8106, https://doi.org/10.1021/ac071181r.

[14] G. Robichaud, J.A. Barry, D.C. Muddiman, IR-MALDESI mass spectrometry imaging of biological tissue sections using ice as a matrix, J. Am. Soc. Mass Spectrom. 25 (2014) 319−328, https://doi.org/10.1007/s13361-013-0787-6.

[15] A. Kiss, D.F. Smith, B.R. Reschke, M.J. Powell, R.M. Heeren, Top-down mass spectrometry imaging of intact proteins by laser ablation ESI FT-ICR MS, Proteomics 14 (2014) 1283−1289, https://doi.org/10.1002/pmic.201300306.

[16] P. Nemes, A.A. Barton, A. Vertes, Three-dimensional imaging of metabolites in tissues under ambient conditions by laser ablation electrospray ionization mass spectrometry, Anal. Chem. 81 (2009) 6668−6675, https://doi.org/10.1021/ac900745e.

[17] C.W. Bacon, D.M. Hinton, T.R. Mitchell, E.R. Palencia, In situ ergot alkaloid detection in three Balansia epichloe-infected grass species, J. Appl. Microbiol. 125 (2018) 976−985, https://doi.org/10.1111/jam.13941.

[18] S.A. Stopka, et al., Metabolic noise and distinct subpopulations observed by single cell LAESI mass spectrometry of plant cells in situ, Front. Plant Sci. 9 (2018) 1646, https://doi.org/10.3389/fpls.2018.01646.

[19] J.A. Barry, et al., Mapping antiretroviral drugs in tissue by IR-MALDESI MSI coupled to the Q Exactive and comparison with LC-MS/MS SRM assay, J. Am. Soc. Mass Spectrom. 25 (2014) 2038−2047, https://doi.org/10.1007/s13361-014-0884-1.

[20] C.W. Bacon, D.M. Hinton, T.R. Mitchell, Screening of Bacillus mojavensis biofilms and biosurfactants using laser ablation electrospray ionization mass spectroscopy, J. Appl. Microbiol. 125 (2018) 867−875, https://doi.org/10.1111/jam.13905.

[21] S.A. Stopka, et al., Ambient metabolic profiling and imaging of biological samples with ultrahigh molecular resolution using laser ablation electrospray ionization 21 Tesla FTICR mass spectrometry, Anal. Chem. 91 (2019) 5028−5035, https://doi.org/10.1021/acs.analchem.8b05084.

[22] M. Nazari, D.C. Muddiman, Cellular-level mass spectrometry imaging using infrared matrix-assisted laser desorption electrospray ionization (IR-MALDESI) by oversampling, Anal. Bioanal. Chem. 407 (2015) 2265−2271, https://doi.org/10.1007/s00216-014-8376-5.

[23] M.T. Bokhart, et al., IR-MALDESI mass spectrometry imaging at 50 micron spatial resolution, J. Am. Soc. Mass Spectrom. 28 (2017), https://doi.org/10.1007/s13361-017-1740-x, 2099-2007.

[24] A. Albert, C. Engelhard, Characteristics of low-temperature plasma ionization for ambient mass spectrometry compared to electrospray ionization and atmospheric pressure chemical ionization, Anal. Chem. 84 (2012) 10657−10664.

[25] L. Imbert, et al., Comparison of electrospray ionization, atmospheric pressure chemical ionization and atmospheric pressure photoionization for a lipidomic analysis of Leishmania donovani, J. Chromatogr., A 1242 (2012) 75−83, https://doi.org/10.1016/j.chroma.2012.04.035.

[26] B. Bartels, et al., Mapping metabolites from rough terrain: laser ablation electrospray ionization on non-flat samples, RSC Adv. 7 (2017) 9045−9050, https://doi.org/10.1039/C6RA26854D.

[27] J.A. Barry, D.C. Muddiman, Global optimization of the infrared matrix-assisted laser desorption electrospray ionization (IR MALDESI) source for mass spectrometry using statistical design of experiments, Rapid Commun. Mass Spectrom. 25 (2011) 3527−3536, https://doi.org/10.1002/rcm.5262.

[28] S.C. Cheng, S.S. Jhang, M.Z. Huang, J. Shiea, Simultaneous detection of polar and nonpolar compounds by ambient mass spectrometry with a dual electrospray and atmospheric pressure chemical ionization source, Anal. Chem. 87 (2015) 1743−1748, https://doi.org/10.1021/ac503625m.

[29] M. Ogawa, A. Kadowaki, T. Yamada, O. Kadooka, Applied Development of a

Novel Fungicide Isotianil (Stout), 2011, pp. 1–15.

[30] (EPA), E. P. A. Vol. 84 FR 58623 (Ed Environmental Protection Agency (EPA)) 58623-58627, Federal Register, Washington, DC, US, 2019.

[31] T.M. Nakanishi, What you can see by developing real-time radioisotope imaging system for plants: from water to element and CO2 gas imaging, J. Radioanal. Nucl. Chem. 318 (2018) 1689–1695, https://doi.org/10.1007/s10967-018-6324-0.

[32] P. Nemes, A.S. Woods, A. Vertes, Simultaneous imaging of small metabolites and lipids in rat brain tissues at atmospheric pressure by laser ablation electrospray ionization mass spectrometry, Anal. Chem. 82 (2010) 982–988, https://doi.org/10.1021/ac902245p.

[33] J. Fideler, S.D. Johanningsmeier, M. Ekelöf, D.C. Muddiman, Discovery and quantification of bioactive peptides in fermented cucumber by direct analysis IR-MALDESI mass spectrometry and LC-QQQ-MS, Food Chem. 271 (2019) 715–723, https://doi.org/10.1016/j.foodchem.2018.07.187.

[34] G.B. Eijkel, et al., Correlating MALDI and SIMS imaging mass spectrometric datasets of biological tissue surfaces, Surf. Interface Anal. 41 (2009) 675–685, https://doi.org/10.1002/sia.3088.

[35] S. Van der Walt, N. Smith, A better default colormap for Matplotlib. http://bids.github.io/colormap, 2015.

[36] J.R. Nuñez, C.R. Anderton, R.S. Renslow, Optimizing colormaps with consideration for color vision deficiency to enable accurate interpretation of scientific data, PLoS One 13 (2018), e0199239, https://doi.org/10.1371/journal.pone.0199239.

[37] F. Carrari, et al., Integrated analysis of metabolite and transcript levels reveals the metabolic shifts that underlie tomato fruit development and highlight regulatory aspects of metabolic network behavior, Plant Physiol. 142 (2006) 1380–1396, https://doi.org/10.1104/pp.106.088534.